Supporting Information for

Improved Strain Engineering of Monolayer Transition Metal Dichalcogenides via van der Waals Epitaxy on Graphene/SiC(0001)

Ryotaro Sakakibara[1,2*], Kaito Hirata[3,4], Yasufumi Takahashi[4,5,6], Wataru Norimatsu[7], and Yasumitsu Miyata[1,2*]

[1] Research Center for Materials Nanoarchitectonics (MANA), National Institute for Materials Science (NIMS), Tsukuba 305-0044, Japan
[2] Department of Physics, Tokyo Metropolitan University, Hachioji, 192-0397, Japan
[3] Department of Physical Science and Engineering, Nagoya Institute of Technology, Nagoya 466-8555, Japan
[4] Department of Electronics, Graduate School of Engineering, Nagoya University, Nagoya 464-8603, Japan
[5] Research Institute for Quantum and Chemical Innovation, Institutes of Innovation for Future Society, Nagoya University, Nagoya 464-8601, Japan
[6] WPI Nano Life Science Institute (WPI-NanoLSI), Kanazawa University, Kanazawa 920-1192, Japan
[7] Faculty of Science and Engineering, Waseda University, Tokyo 169-8555, Japan

*Correspondence should be addressed to R.S. (SAKAKIBARA.Ryotaro@nims.go.jp) and Y.M. (MIYATA.Yasumitsu@nims.go.jp)

Contents

Experimental details

Preparation of graphene/SiC substrate

A nominally on-axis 4H-SiC(0001) substrate (CREE inc.) was cleaned by ultrasonication in acetone and ethanol, and then immersed in a hydrofluoric acid solution to remove the oxide layer on the surface. The pre-treated SiC substrate was then annealed at 1720°C for several minutes in an Ar gas flow atmosphere at a flow rate of 100 sccm. This process resulted in the formation of 1–2 layers of epitaxial graphene over the entire substrate surface.[1,2]

CVD growth of WSe_2 and MoS_2

Salt-assisted CVD growth was conducted using a two-zone electric furnace.[3-5] For WSe_2 growth, a ceramic boat containing Se beads was placed upstream, while KBr powder (25 mg), WO_3 powder (25 mg), and a growth substrate were positioned downstream inside a quartz tube. The quartz tube was filled with a N_2/H_2 gas mixture (0.1% H_2) at a flow rate of 500 sccm. The upstream and downstream furnaces were heated to 420°C and 840°C, respectively, and maintained at these temperatures for 2 min. The system was then rapidly cooled to room temperature using an electric fan. For MoS_2 growth, S flakes, KBr powder (3 mg), and MoO_2 powder (30 mg) were used as precursors. The upstream and downstream furnaces were set to 180°C and 780°C, respectively. N_2 carrier gas was supplied at a flow rate of 250 sccm and the growth duration was 3 min.

Characterizations

PL and Raman measurements were carried out at room temperature using a Renishaw inVia spectrometer. A 532 nm excitation laser with a spot size of about 1 μm^2 was used. Cross-sectional STEM observation was carried out using a JEM-ARM200F microscope operated at an acceleration voltage of 200 kV. HAADF imaging and EDS measurements were performed. A thin specimen for observation was prepared using the focused ion beam method. To evaluate the catalytic reactivity of the MoS_2 samples, HER measurements were carried out using a home-made SECCM.[6] HER current mapping images were acquired in hopping mode, with a nanopipette aperture radius of about 50 nm. The threshold current for distance control between the nanopipette and the sample, as well as the hopping amplitude, were set to 0.3 pA and 1 μm, respectively. Further details of the HER measurements are provided in the previous study.[6] Atomic force microscopy (AFM) observation was carried out in the dynamic force mode to obtain topographic images of the sample surfaces.

Supplementary notes

Strain direction in monolayer WSe_2

The strain in our synthetic WSe_2 monolayers is considered isotropic rather than uniaxial, for the following two reasons. First, WSe_2 grown on graphene/SiC shows no evidence of E' mode splitting in the Raman spectra (Figure S5), which is a feature typically associated with uniaxial strain.[7] Second, the in-plane TEC of SiC is isotropic, owing to the three-fold symmetry of the atomic arrangement on the SiC(0001) plane. The same reasoning applies to WSe_2 grown on other substrates, including graphite, SiO_2, and sapphire. It is worth noting that directional strain control may be possible by using substrates with anisotropic TEC.

On the limitation of wavenumber resolution in our Raman spectroscopy setup

As described in the main text, the effect of strain in WSe_2 is clearly observed using PL measurements, while it is difficult to detect using Raman spectroscopy. Specifically, the E' mode of WSe_2 on graphene/SiC exhibited nearly uniform characteristics across the grain, and its Raman shift is indistinguishable from that of WSe_2 on graphite (Figures S4 and S5). According to a previous study, the Raman shift rate induced by biaxial tensile strain is approximately -1 $cm^{-1}/\%$.[8] Therefore, for the estimated 0.4% strain in our WSe_2/graphene/SiC sample, a Raman shift of around 0.4 cm^{-1} would be expected. This shift is comparable to the wavenumber resolution of our current setup (~0.4 cm^{-1}), making it difficult to resolve such small shifts. Higher-resolution measurements using finer gratings may allow for a more accurate strain evaluation.

In contrast, for MoS_2 grown on graphene/SiC, a clear shift of the E' mode relative to that on graphite is observed (Figure S12). This can be attributed to the higher strain sensitivity of the E' mode in MoS_2, which exhibits a Raman shift rate of approximately -4 $cm^{-1}/\%$.[8]

Origin of the interaction between TMDs and graphene/SiC substrate

As mentioned in the main text, a strong interaction between TMDs and substrate is necessary to introduce thermal strain. Here, we discuss a possible origin of the interaction between TMDs and graphene/SiC substrate. One possible scenario is the formation of covalent bonds between dangling bonds at the TMD edges and reactive sites on the underlying graphene or SiC. Specifically, TMD edges may be bound to graphene defects generated during the CVD process, or to SiC surface dangling bonds exposed through holes in graphene layer. These local anchor points could mediate strain transfer upon cooling.

Effect of the step-terrace structure and graphene layer on the PL properties of WSe_2

Figure S7 shows AFM topography images of WSe_2 grown on graphene/SiC. The step-terrace structure of the SiC substrate surface is clearly observed,[1] and the WSe_2 grains covered multiple steps with heights of 2–5 nm. Here, the PL peak energy and FWHM maps of WSe_2 shown in Figures 2b and 2c of the main text do not exhibit any distribution correlated with the step-terrace structure. This indicates that the strain distribution is not related to the underlying morphology. In contrast, the PL intensity map in Figure 2a of the main text shows regions with lower intensity. As shown in Figure S8, this intensity distribution appears to correlate with the FWHM map of the graphene 2*D* band. Since the FWHM of the 2*D* band positively correlates with the number of graphene layers,[9,10] it is suggested that the PL intensity of WSe_2 tends to decrease on regions with fewer graphene layers.

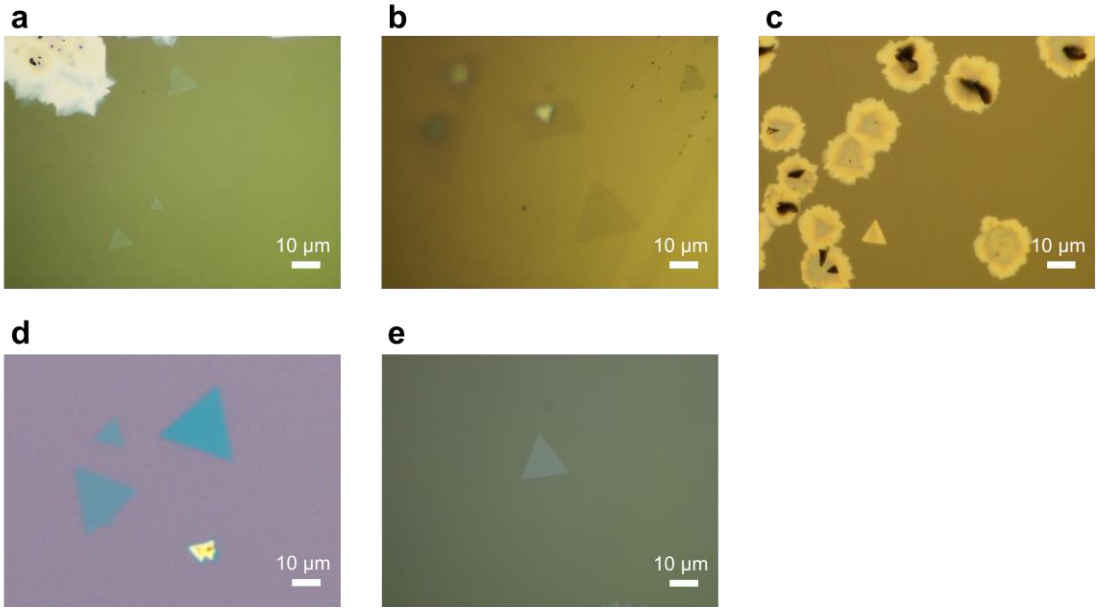

Figure S1. Optical images of WSe_2 crystals grown on (a) graphene/SiC, (b) graphite, (c) bare SiC, (d) SiO_2, and (e) sapphire substrates.

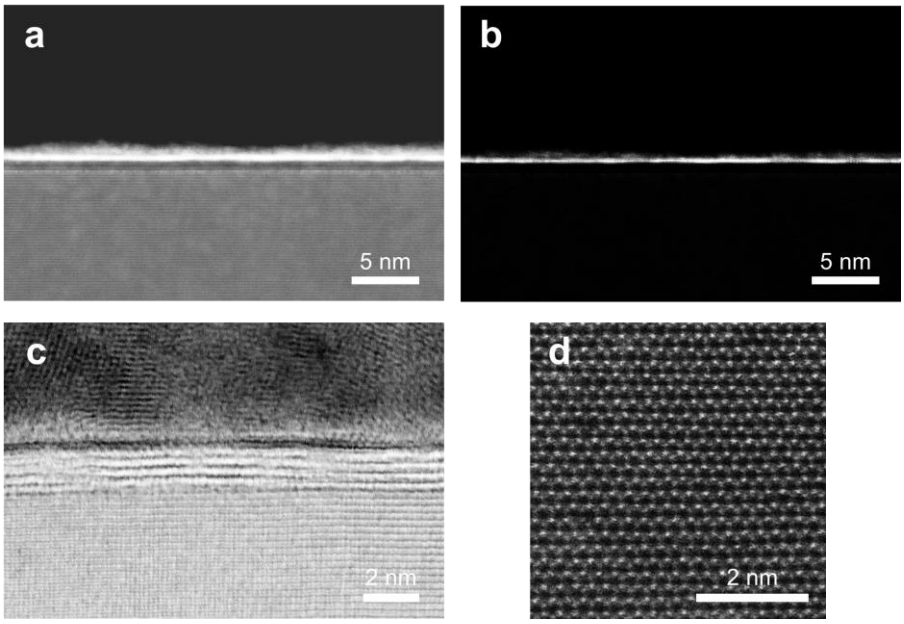

Figure S2. (a) Cross-sectional HAADF-STEM image of WSe_2/graphene/SiC. (b) HAADF-STEM image of the same field of view as (a) with reduced contrast. (c) Bright-field STEM image of the same sample. (d) In-plane view of the WSe_2 lattice, initially grown on an SiO_2/Si substrate and later transferred onto a TEM grid.

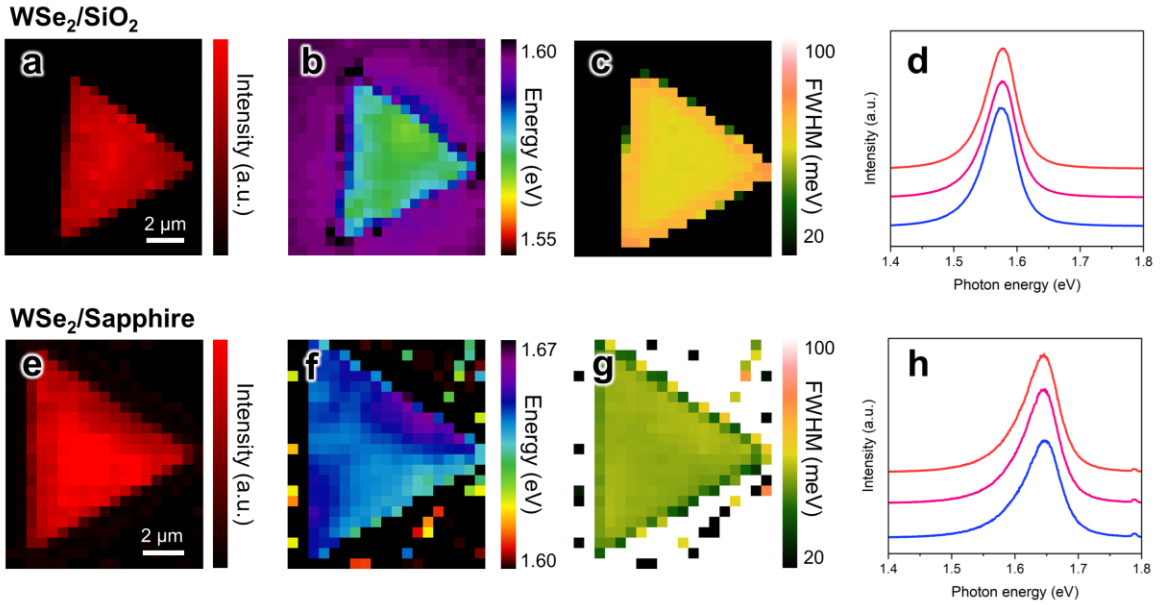

Figure S3. (a) PL intensity, (b) peak energy, and (c) peak FWHM maps of monolayer WSe_2/SiO_2. (d) PL spectra measured at three different points. (e) PL intensity, (f) peak energy, and (g) peak FWHM maps of monolayer WSe_2/sapphire. For the PL peak of monolayer WSe_2/sapphire, a peak derived from charged exciton (trion) is prominent on the low-energy side, so the spectrum was fitted with two Voigt function components.[11] The map data are for the neutral free exciton. (h) PL spectra measured at three different points.

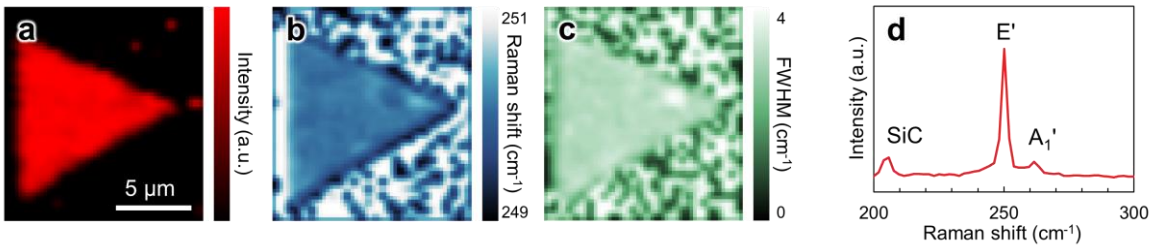

Figure S4. (a) E' Raman mode intensity, (b) Raman shift, and (c) FWHM maps of monolayer WSe_2 grown on graphene/SiC. (d) Typical Raman spectrum of monolayer WSe_2 grown on graphene/SiC.

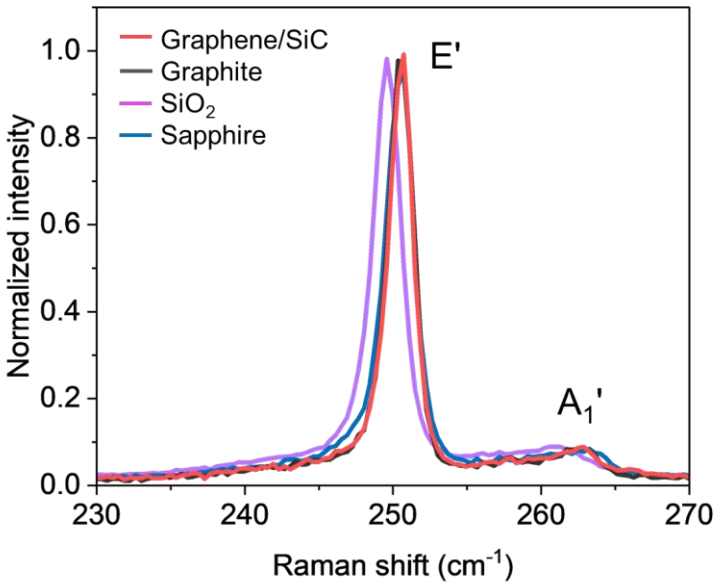

Figure S5. Typical Raman spectra of monolayer WSe_2 grown on graphene/SiC, graphite, SiO_2, and sapphire substrates. Raman shift due to tensile strain was recognized only on SiO_2.

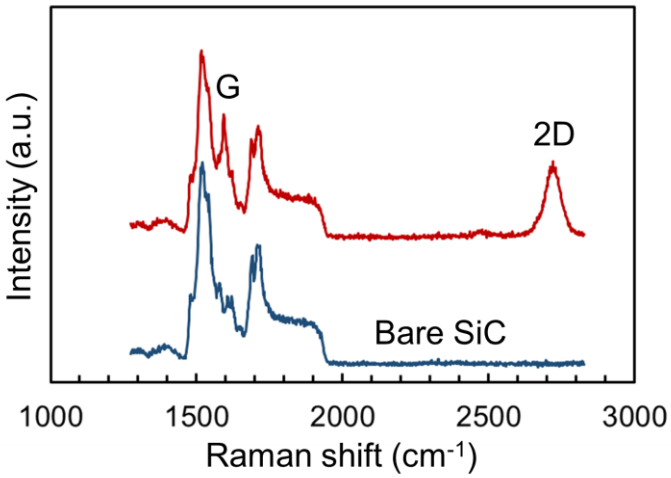

Figure S6. Raman spectra of graphene/SiC after the CVD growth of WSe_2 (top) and a bare SiC substrate for reference (bottom).

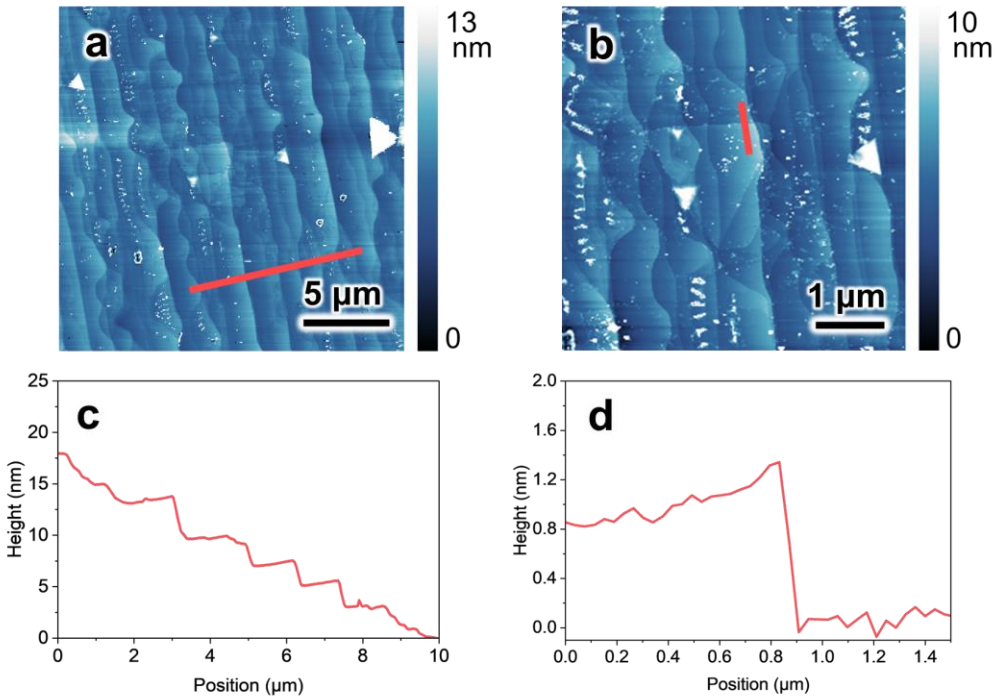

Figure S7. (a,b) AFM topography images of WSe_2 crystals grown on graphene/SiC. (c,d) Height profiles acquired along the red lines in (a) and (b), respectively. The step-terrace structure of the SiC substrate surface is clearly visible. In (d), the thickness of monolayer WSe_2 (~0.8 nm) is confirmed. The finger-like structures can also be seen, which may have formed during thermal decomposition of SiC.[12]

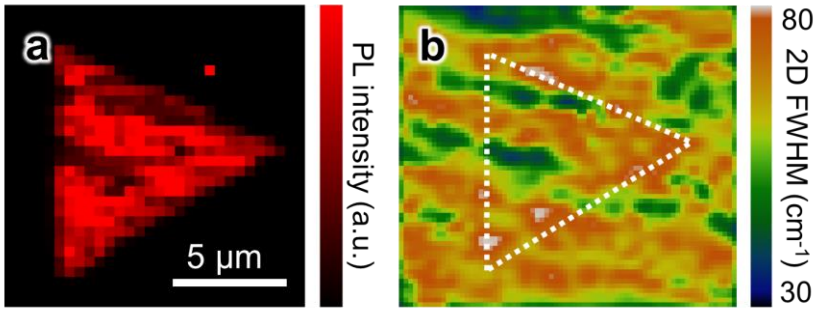

Figure S8. (a) PL intensity map of monolayer WSe_2 grown on graphene/SiC. (b) Raman FWHM map of the graphene 2*D* band acquired in the same region as (a), where the position of the WSe_2 crystal is outlined by dashed lines. By comparing the two map images, it can be said that the inhomogeneity of the PL intensity correlates with the 2*D* FWHM, which reflects the number of graphene layers.[9,10]

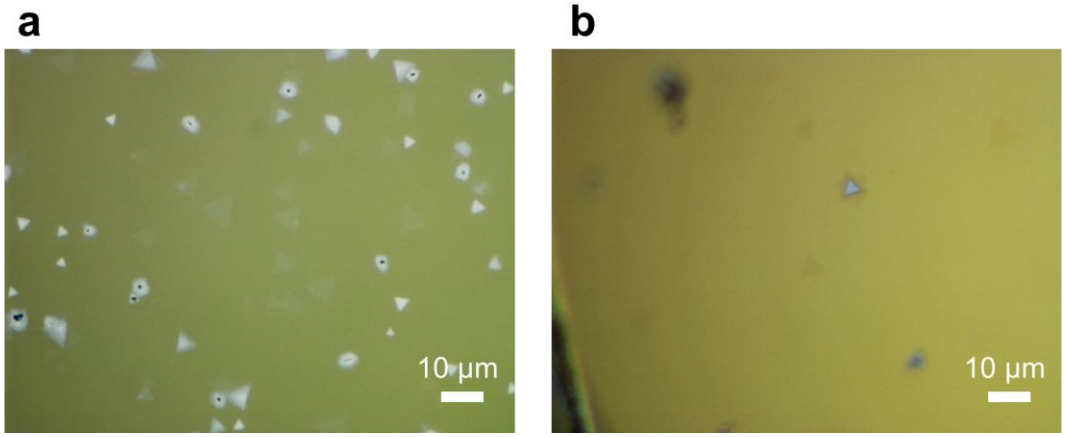

Figure S9. Optical images of MoS_2 crystals grown on (a) graphene/SiC and (b) graphite substrates.

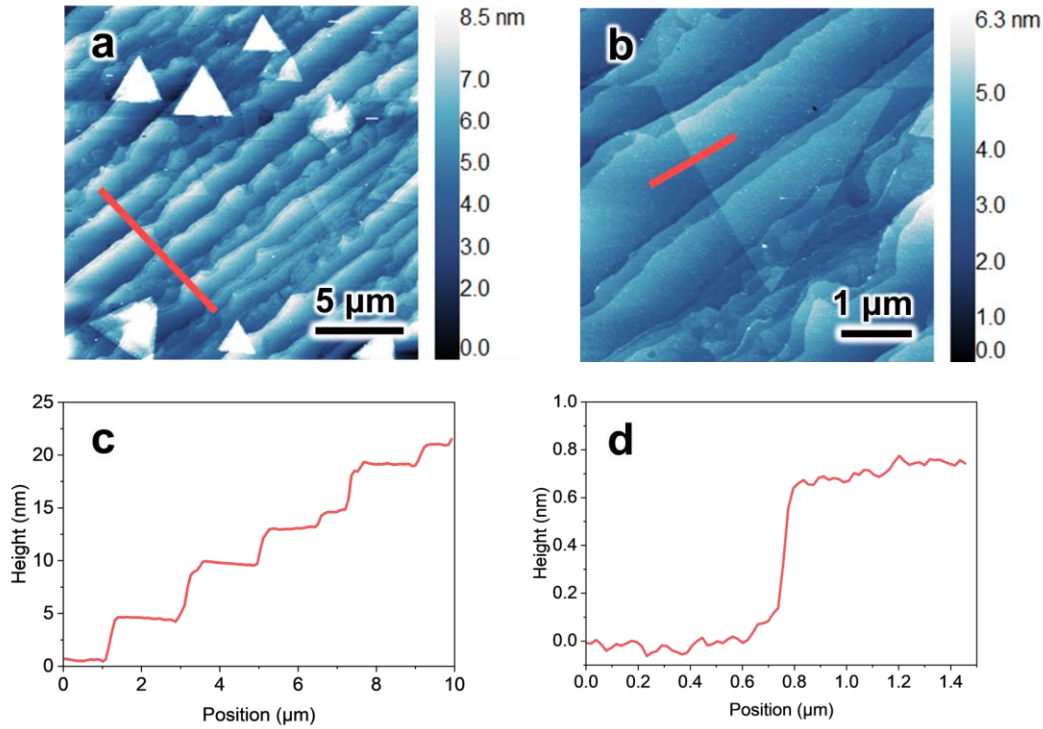

Figure S10. (a,b) AFM topography images of MoS_2 crystals grown on graphene/SiC. (c,d) Height profiles acquired along the red lines in (a) and (b), respectively. In (d), the thickness of monolayer MoS_2 (~0.7 nm) is confirmed.

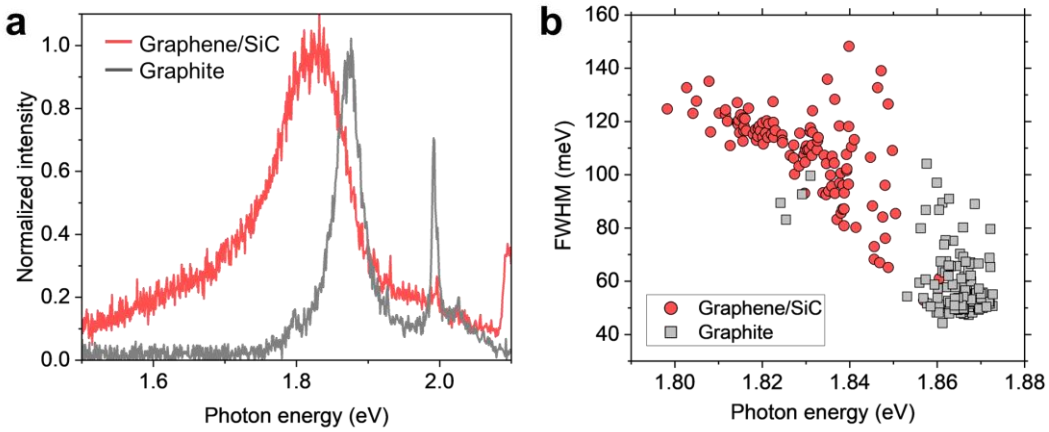

Figure S11. (a) Typical PL spectra and (b) plot of PL peak FWHM versus peak energy for monolayer MoS_2 grown on graphene/SiC and graphite. In contrast to the case of WSe_2, tensile-strained MoS_2 shows a broadening of linewidth with a redshift of the PL peak. This behavior can be explained by enhanced intervalley scattering arising from strain-induced band structure modulation in MoS_2.[13,14]

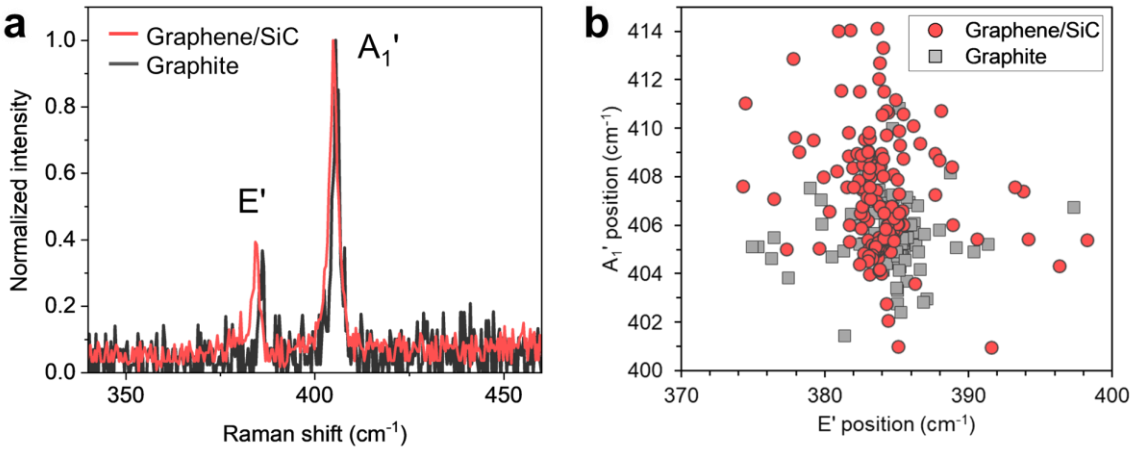

Figure S12. (a) Typical Raman spectra and (b) Plot of Raman A_1' position versus E' position for monolayer MoS_2 grown on graphene/SiC and graphite. The slight redshift of the E' mode in monolayer MoS_2 on graphene/SiC indicates the presence of tensile strain.[15]

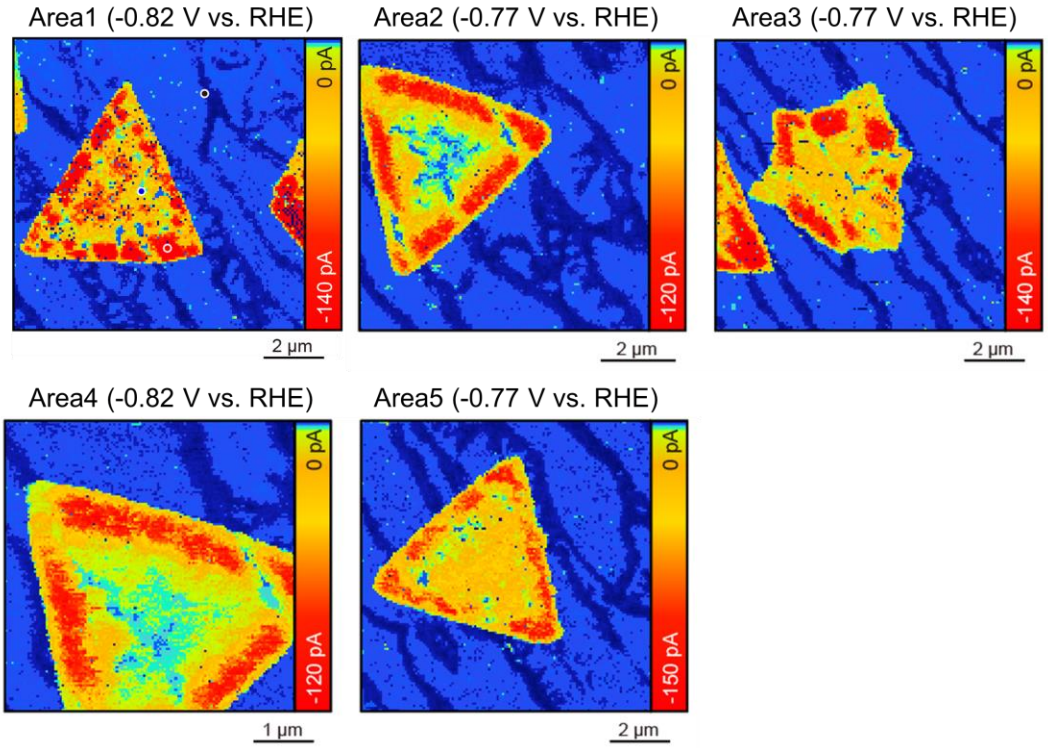

Figure S13. HER current mapping images for various monolayer MoS_2 grains grown on graphene/SiC. The prominent catalytic activity was observed for all the grains.

REFERENCES

(1) Norimatsu, W.; Kusunoki, M. Epitaxial graphene on SiC{0001}: advances and perspectives. *Phys. Chem. Chem. Phys.* **2014**, *16*, 3501-3511.

(2) Kusunoki, M.; Norimatsu, W.; Bao, J.; Morita, K.; Starke, U. Growth and Features of Epitaxial Graphene on SiC. *J. Phys. Soc. Jpn.* **2015**, *84*, 121014.

(3) Kobayashi, Y.; Sasaki, S.; Mori, S.; Hibino, H.; Liu, Z.; Watanabe, K.; Taniguchi, T.; Suenaga, K.; Maniwa, Y.; Miyata, Y. Growth and Optical Properties of High-Quality Monolayer WS_2 on Graphite. *ACS Nano* **2015**, *9*, 4056-4063.

(4) Wada, N.; Pu, J.; Takaguchi, Y.; Zhang, W.; Liu, Z.; Endo, T.; Irisawa, T.; Matsuda, K.; Miyauchi, Y.; Takenobu, T.; Miyata, Y. Efficient and Chiral Electroluminescence from In-Plane Heterostructure of Transition Metal Dichalcogenide Monolayers. *Adv. Funct. Mater.* **2022**, *32*, 2203602.

(5) Ogura, H.; Kawasaki, S.; Liu, Z.; Endo, T.; Maruyama, M.; Gao, Y.; Nakanishi, Y.; Lim, H. E.; Yanagi, K.; Irisawa, T.; Ueno, K.; Okada, S.; Nagashio, K.; Miyata, Y. Multilayer In-Plane Heterostructures Based on Transition Metal Dichalcogenides for Advanced Electronics. *ACS Nano* **2023**, *17*, 6545-6554.

(6) Takahashi, Y.; Kobayashi, Y.; Wang, Z.; Ito, Y.; Ota, M.; Ida, H.; Kumatani, A.; Miyazawa, K.; Fujita, T.; Shiku, H.; Korchev, Y. E.; Miyata, Y.; Fukuma, T.; Chen, M.; Matsue, T. High-Resolution Electrochemical Mapping of the Hydrogen Evolution Reaction on Transition-Metal Dichalcogenide Nanosheets. *Angew. Chem. Int. Ed.* **2020**, *59*, 3601-3608.

(7) Dadgar, A. M.; Scullion, D.; Kang, K.; Esposito, D.; Yang, E. H.; Herman, I. P.; Pimenta, M. A.; Santos, E. J. G.; Pasupathy, A. N. Strain Engineering and Raman Spectroscopy of Monolayer Transition Metal Dichalcogenides. *Chem. Mater.* **2018**, *30*, 5148-5155.

(8) Michail, A.; Yang, J. A.; Filintoglou, K.; Balakeras, N.; Nattoo, C. A.; Bailey, C. S.; Daus, A.; Parthenios, J.; Pop, E.; Papagelis, K. Biaxial Strain Transfer in Monolayer MoS_2 and WSe_2 Transistor Structures. *ACS Applied Materials & Interfaces* **2024**, *16*, 49602-49611.

(9) Ferrari, A. C. Raman spectroscopy of graphene and graphite: Disorder, electron–phonon coupling, doping and nonadiabatic effects. *Solid State Commun.* **2007**, *143*, 47-57.

(10) Graf, D.; Molitor, F.; Ensslin, K.; Stampfer, C.; Jungen, A.; Hierold, C.; Wirtz, L. Spatially resolved Raman spectroscopy of single- and few-layer graphene. *Nano Lett.*

2007, *7*, 238-242.

(11) Chae, W. H.; Cain, J. D.; Hanson, E. D.; Murthy, A. A.; Dravid, V. P. Substrate-induced strain and charge doping in CVD-grown monolayer MoS_2. *Appl. Phys. Lett.* **2017**, *111*, 143106.

(12) Bolen, M. L.; Harrison, S. E.; Biedermann, L. B.; Capano, M. A. Graphene formation mechanisms on 4H-SiC(0001). *Phys. Rev. B* **2009**, *80*, 115433.

(13) Niehues, I.; Schmidt, R.; Druppel, M.; Marauhn, P.; Christiansen, D.; Selig, M.; Berghauser, G.; Wigger, D.; Schneider, R.; Braasch, L.; et al. Strain Control of Exciton-Phonon Coupling in Atomically Thin Semiconductors. *Nano Lett.* **2018**, *18*, 1751-1757.

(14) Khatibi, Z.; Feierabend, M.; Selig, M.; Brem, S.; Linderälv, C.; Erhart, P.; Malic, E. Impact of strain on the excitonic linewidth in transition metal dichalcogenides. *2D Mater.* **2019**, *6*, 015015.

(15) Michail, A.; Delikoukos, N.; Parthenios, J.; Galiotis, C.; Papagelis, K. Optical detection of strain and doping inhomogeneities in single layer MoS_2. *Appl. Phys. Lett.* **2016**, *108,* 173102.